Advances in Materials Research, *Vol. 7 No. 2 (2018) 105-118*
DOI: https://doi.org/10.12989/amr.2018.7.2.105

Effect of grain refinement on the performance of AZ80 Mg alloys during wear and corrosion

Gajanan M Naik*[1], Gopal D. Gote[2], Narendranath S[1] and S.S. Satheesh Kumar[3]

[1]*Dept. of Mechanical Engineering, NITK, Surathkal, Mangalore 575025, Karnataka, India*
[2]*Dept. of Mechanical Engineering, IITB, Mumbai 400 076, Maharashtra, India*
[3]*Defence Metallurgical Research Laboratory, Hyderabad 500058, Telangana, India*

(*Received August 20, 2018, Revised February 25, 2019, Accepted February 26, 2019*)

Abstract. Magnesium and its alloys are attracted towards all engineering applications like automotive, marine, aerospace etc. due to its inherent high strength to weight ratio. But, extensive use of Mg alloys is limited to the current scenario because of low wear and corrosion resistance behavior. However, equal channel angular press is one of the severe plastic deformation technique which has been effective method to improve the wear and corrosion resistance by achieving fine grain structure. In this study, the effect of grain refinement on wear and corrosion resistance of AZ80 Mg alloys were investigated. The wear behavior of the coarse and fine-grained Mg alloys was examined through L_9 orthogonal array experiments in order to comprehend the wear behavior under varies control parameters. It was shown that ECAPed alloy increased the wear and corrosion resistance of the Mg alloy through the formation of fine grain and uniform distribution of secondary β- phase. Also, the performance of AZ80 Mg alloy for these changes was discussed through SEM morphology.

Keywords: AZ80; ECAP; grain refinement; wear; corrosion

1. Introduction

The major concern of this century is to reduce the CO_2 emission and environmental pollution. In this regard, the magnesium alloys play an important role to fulfill these demands because of its lower density and higher strength to weight ratio. Concerning density of magnesium alloys, it is lightest among all engineering materials which is 37.03% lighter than aluminium and 78.37% lighter than steel (Mustafa *et al*. 2008). Therefore magnesium alloys are promising alternatives of aluminium alloys and steels for the manufacture of all engineering parts (Esmaily *et al*. 2017). However, their poor ductility, difficult to formability, lower wear and corrosion resistance properties were limit its extensive usage in industries (Gray *et al*. 2002). Especially, their unsatisfactory wear and corrosion behavior are restricted the use of Mg alloys. (Bettles *et al*. 2005) have discussed the strengths and weakness of Mg alloys. Currently, many researchers have been working on the growth of Mg alloys and to encounter aforementioned problems.

Zhang *et al*. (2007) have investigated the wear and corrosion performance of AZ91D Mg alloy

*Corresponding author, Ph.D., E-mail: gajamnaik@gmail.com

 ISSN: 2234-0912 (Print), 2234-179X (Online)

with and without micro-arc oxidation (MAO) coating in Hank's solution, from the study it was concluded that the corrosion and wear properties of the AZ91D Mg alloy was improved after MAO coating compare to uncoated sample. Here the corrosion potential was enhanced from –1.578 V to –0.430 Majumdar *et al*. (2003) reported the effect of laser surface melting on hardness, corrosion and wear behavior of MEZ Mg alloy (Zn 0.5%, Mn 0.1%, Zr 0.1%, rare earth (RE) elements 2%, remaining percentage Mg). It was found that micro-hardness of the laser treated surface was improved from 35VHN to 85VHN, wear and corrosion resistance of the laser surface melted MEZ, significantly enhanced in a 3.56 wt.% NaCl solution due to grain refinement and re-distribution of the intermetallic phases. Hence, from the literature, it was examined that the corrosion and wear resistance can be improved through surface treatment. But, the obtained results are limited to surface-treated layer. Thereby, it is believed that the wear and corrosion resistance of magnesium alloys intensely improved by grain refinement and distribution of secondary phases throughout the material, which can be achieved by one of the promising severe plastic deformation (SPD) technique that is equal channel angular pressing (ECAP).

In this study, a Taguchi's L_9 (3^4) orthogonal array table was used to optimize the wear experiments. Four controlling input factors with three levels for each parameter was selected. The wear rate and co-efficient of friction are selected as quality response objectives. Based on the Taguchi mean effect plots effect of inputs on the output responses were analyzed and an optimal setting parameter was identified. Also, the DoE method is utilized to obtain most influencing factor and percentage contribution was analyzed through the analysis of variance (ANOVA). Further, in order to understand the wear mechanisms, the worn surfaces of the pin were observed through scanning electron microscope. On the other hand corrosion behavior of coarse and fine-grained Mg alloys after ECAP were investigated by electrochemical corrosion analyzer.

2. Experimental details

2.1 Materials and processing

The experiments were accompanied using a wrought AZ80-Mg alloy purchased from Exclusive magnesium Pvt. Ltd. Hyderabad, India, having an elemental composition, in wt.%, of Al-8%, Zn-0.5%, Mg-91.5%. The specimens of the as-received wrought AZ80 Mg material with diameter 20 mm and length 200 mm were processed by ECAP up to 4 passes using an ECAP die having a channel angle (Φ) 110° and an outer arc of curvature (Ψ) of 30°. This process, imposes an equivalent strain of ~ 0.74 in each pass and the ECAP processing was performed at 350^0C using route Bc where the specimen is rotated by 90° in counter clockwise direction between consecutive passes at a ram speed of 1mm/s. The ECAP carried out at 350ºC in order to avoid problems with surface cracking at lower temperatures. Prior to ECAP, the specimens were subjected to a diffusion annealing treatment at 400ºC for 18h by keeping in a furnace to achieve uniform distribution of secondary elements (β-phase) in Mg matrix and molybdenum-disulfide (MoS_2) was used on the ECAP channel surface and specimen to avoid frictional resistance between die and sample. The phase identification and microstructural observation was explored by Optical microscopy (BIOVIS material plus) and Scanning Electron Microscopy (Model: JEO JSM–638OLA from JEOL, USA) coupled with an Energy-dispersive X-ray spectroscopy (EDS). The Microhardness is measured using Micro-hardness testing machine M/s OMNI TECH, PUNE, make MVH–S–AUTO by applying a load of 100gm for a dwell time of 13 s. The X-ray diffraction

Table 1 Selected wear parameters

Control parameters	Symbol	Levels		
		Low	Medium	High
Material	A	As-received (A1)	ECAP-2P (A2)	ECAP-4P (A3)
Applied Load (N)	B	10	20	30
Sliding distance (m)	C	1500	3000	4500
Sliding velocity(m/s)	D	1	2	3

measurements are carried out in M/s Proto Manufacturing Ltd., CANADA make PROTO– iXRD MGR40 wherein the analysis was carried out 2θ: angular range of 20º - 90º at a scanning speed of 2 ^{0}/min.

2.2 Wear and corrosion

Dry sliding wear test was carried out by varying load from 10N to 30N with an increment of 10 N and sliding distance 1500 m to 4500 m with an increment of 1500 m, sliding velocity 1 m/s, 2 m/s, and 3 m/s were selected. Throughout the test, coarse, fine and ultra-fine grained magnesium alloy was considered as working material. This study gives an attention to four parameters and each parameter have three levels which are shown in Table 1. Table 2 presents L9 experimental design and responses, which was planned according to the design of experiments (DoE). This is employed to simplify the experiments and to reduce testing time (Jeong-Lian *et al*. 2009, Shetty *et al*. 2017, Naik *et al*. 2017, Naik *et al*. 2018). The billet dimensions of 10mm diameter and 20mm length were prepared as per ASTMG99-05 and wear tests were accomplished at room temperature using pin-on-disc wear tester (DUCOM-TR-20LE-PHM 400-CHM 600, Instruments, Bangalore, India). Experiments were carried out on rigid and polished disc (EN31 steel, Ducom Instruments) with hardness 65 HRC. Prior to wear experiment, the specimen was polished with SiC emery papers of 1000 and 2000 grit, followed by cleaned for 5-10 min and lastly dried. The losses of mass were determined from the differences in weight of samples estimated before and after the wear test using a precision balance of 0.001 g accuracy. Volumetric wear loss of material was calculated by dividing the mass loss by the mass density of the Mg alloy (1.7 g/cm^3). Volumetric wear rate was estimated by dividing the volumetric wear loss by sliding distance. Each test was carried out thrice in order to check the reproducibility and an average of three tests were taken to calculate the wear rate (Mitsuhiro *et al*. 2013).

The corrosion study was carried out using Electrochemical Corrosion Analyzer (ECA), model: Gill AC-1684, supplied by Tech-science Pvt Limited, Pune (India) with a reference electrode saturated calomel electrode (SCE) and an auxiliary electrode graphite (Gr). 1 cm^2 area of the working electrode was exposed to the 3.5 wt.% NaCl solution. Prior to corrosion test, specimens were polished with 400, 600, 800, 1000, 1200, 1500, 2000 grit emery papers (SiC) and cleaned with ethanol. The specimens were kept in corrosion cell kit in the 3.5 Wt.% sodium chloride solution for 30 min to reach steady open circuit potential (OCP). Further, the Electrochemical Impedance spectroscopy (EIS) test of starting frequency 100 kHz and ending frequency 10 mHz with a scan speed of 2 mV/s was carried on the electrochemical corrosion analyzer. The surface morphology of the corroded sample was observed through SEM.

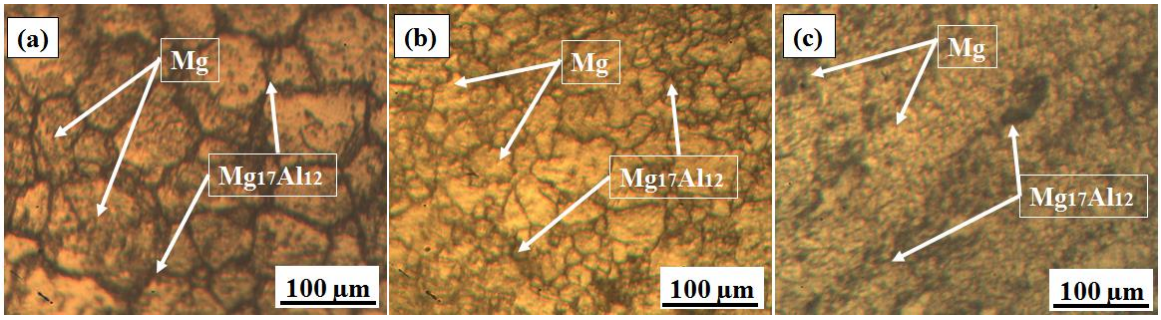

Fig. 1 Optical microscopy image of a) as-received b) ECAP-2Pass and c) ECAP-4Pass

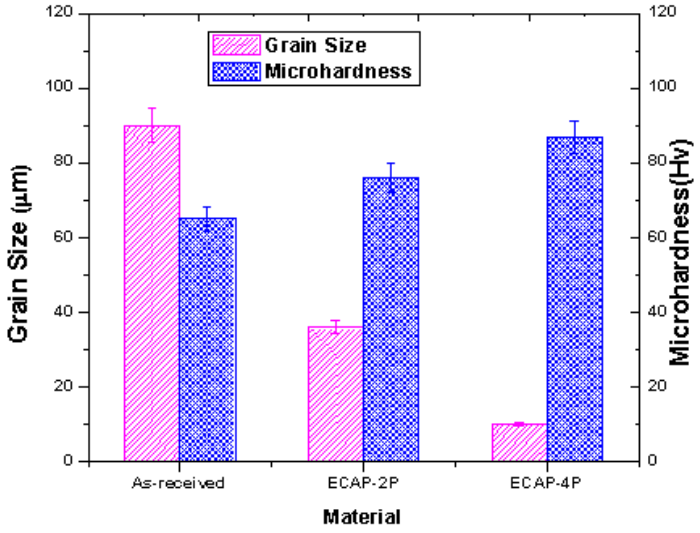

Fig. 2 Grin size and Micro-hardness of as-received and ECAP processed samples

3. Results and discussion

3.1 Microstructure and microhardness

Optical microscopic image of as-received and ECAP processed samples are presented in Fig. 1(a-c). The approximate average grain size of as-received, ECAP-2P and ECAP-4P processed AZ80 alloy was estimated to be 50 µm. 36 µm and 11 µm respectively. The microstructure of ECAP two pass and four pass sample showed the homogeneous distribution of grains and secondary phases ($Mg_{17}Al_{12}$) and the precipitates were observed at the grain boundaries which was confirmed through X-ray diffraction analysis as revealed in Fig. 9 (a-c). The average grain size and Micro-hardness plot in Fig. 2. Shows that ECAP processes showed decreased the grain size due to dynamic recrystallization and increased micro-hardness because of induced equivalent plastic strain and work hardening during the process. Also, the homogeneous precipitation of secondary particles contributes towards higher micro-hardness and act as a corrosion barrier (Mustafa *et al*. 2012).

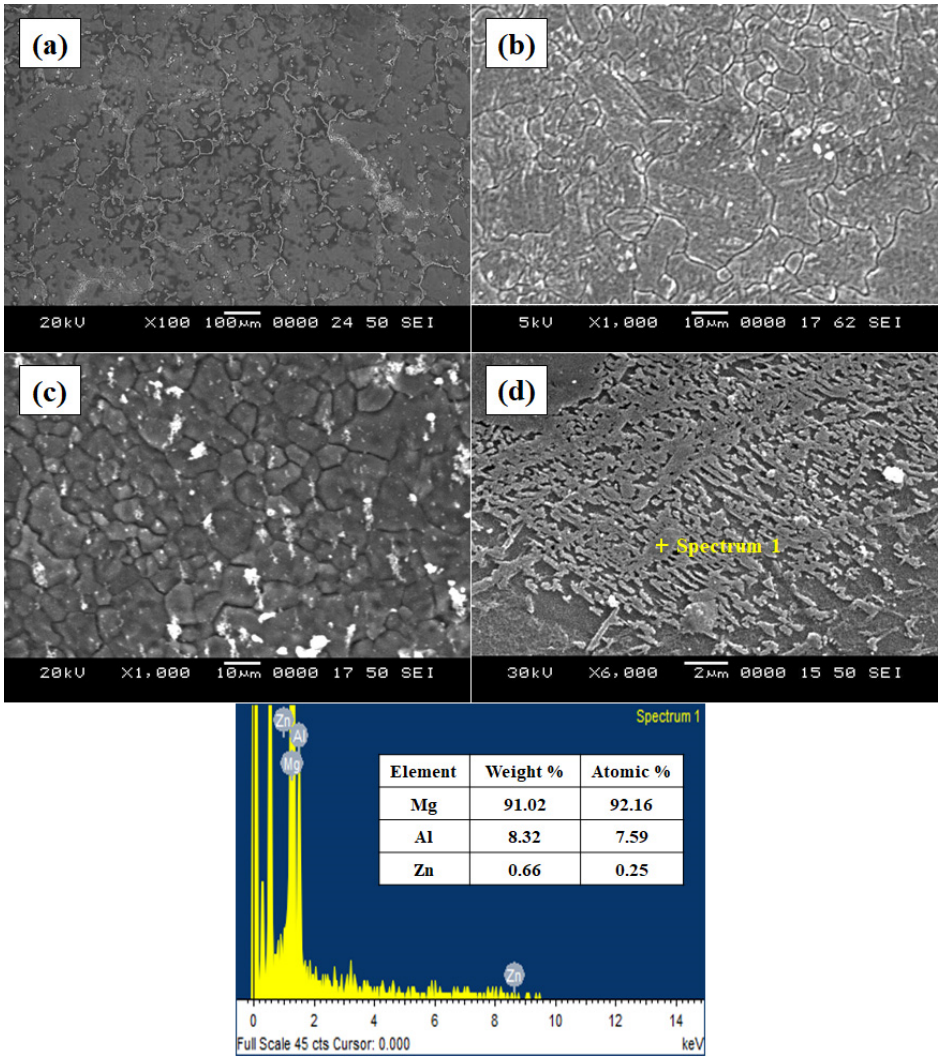

Element	Weight %	Atomic %
Mg	91.02	92.16
Al	8.32	7.59
Zn	0.66	0.25

Fig. 3 SEM images of a) as-received b) ECAP-2Pass and c) ECAP-4Pass d) Precipitation of secondary phase after ECAP-4P with EDS analysis

3.2 SEM analysis

Fig. 3 shows the microstructure evolution of the AZ80 Mg alloy in the as-received and after ECAP for 2, and 4 passes. It can be observed, the ECAP-2P, 4P microstructures consist of bimodal and equiaxed grains depicted in fig 3 (b) and (c) respectively. Indicating that dynamic recrystallization (DRX) has occurred (Gajanan *et al*. 2019, Mustafa *et al*. 2012). The uniformity of grains is improved by successive breaking up of coarse grains after 4 passes of ECAP, the grains becomes uniform with a mean grain size of 11µm as shown in fig 3 (c). Further, microstructure observation was carried out on the ECAP-4P sample provides direct evidence of the precipitates of $Mg_{17}Al_{12}$ in the Mg matrix. A precipitate was present after the ECAP-4P as shown in fig 3 (d) which was confirmed through the EDS results.

3.3 Wear rate and coefficient of friction

In this work, nine no. of experiments have been completed to analyze the effect of control parameters on the wear rate and frictional coefficient using the pin-on-disc wear tester. The experimental design and results are presented in Table 2. Fig. 4. Indicates mean effect plots of wear rate and coefficient of friction to explore the impact of control factors on responses. From Fig. 4. It was observed that volume loss caused by wear noticeably decreased with decreasing grain size. This was evidently proved while comparing wear rate of as-received alloy with ECAP-2 pass results. The reduction of wear rate is because of ECAP process which affords better micro-hardness results due to grain refinement. This is also proved through Hall-Petch relationship associated with the hardness and the relationship between wear loss and hardness interpreted by Holms and Archards adhesive wear theory (Bolin *et al*. 2017). This show improved wear resistance property of ECAP processed AZ80 Mg alloy. Grain refinement brings an improvement in the wear resistance as compared with as-received AZ80 magnesium alloy. On the other hand, ultra-fine grained ECAP-4P processed material exhibited higher wear loss compare to ECAP-2P this is may be due to grain boundary sliding effect (Yoshida *et al*. 2002). With increase of applied load and sliding distance the wear rate increases indicating the influence of applied load and sliding distance on wear rate and coefficient of friction (C.o.F). This is attributed to the detachment of the pin surface in the form of delamination and adhesion to the increment of local temperature. Taltavull *et al*. (2013) have made a similar observation on AM60B magnesium alloy (Taltavull *et al*. 2013). Hence, the present study also agrees that the wear behavior of unprocessed and ECAP processed Mg alloy increases with the increase in the applied load. When the applied load on the pin (AZ80) is increased, the area of interaction would increase towards the disc area, resulting in increased frictional force between two sliding surfaces i.e pin and disc. The increased frictional force between the interface of pin and disc carry higher wear. Hence, higher wear rate was obtained by increasing load. The effect of sliding distance on wear loss and coefficient of friction was observed from mean effect plot. Here, with the increase in sliding distance from 1500m to 4500m, the wear rate increases. This behavior illustrates that further increase of sliding distance increases the wear rate of the Mg alloy. Correspondingly, by increasing sliding distance increase in surface temperature is inevitable, resulting in thermal softening of material cause higher wear loss which leads to oxidation wear mechanism. The fourth influencing control factor is sliding speed. From the observation over the mean effect plot, it is evident that the wear rate of the Mg alloy decreases with the increase of sliding speed from 1m/s to 2m/s initially, and for further increase in sliding speed from 2m/s to 3m/s. the wear rate of the Mg alloy is higher associated with that of the former. Thus, the transition from low to severe wear was observed. Also, the friction coefficient is analyzed under four different control parameters and behaviors were observed through mean effect plot depicts in Fig. 4 (a-d). It can be observed similar trend as wear rate. The friction produced owing to the relative motion between pin and disc is the ratio of frictional force generated during dry sliding tests to applied normal load on the surface. Hence for all experimental conditions, the coefficient of friction of the Mg alloy is much smaller it varied from 0.1-0.3. The association between the coefficient of friction (C.o.F) and sliding distance for the experimental trial #3, #5 and #7 of Table 2 depicts in Fig. 5. Curve 1 of Fig. 5 represents the variation of coefficient of friction under condition A1B3C3D3 (i.e., Expt. No. 3 of Table 2), the wear rate is 0.0254mm^3/m and coefficient of friction is 0.3. Curve 2 of Fig. 5 illustrates the friction coefficient variation under condition A2B2C3D1 (i.e., Expt. No. 5 of Table 2), where the wear rate is 0.0102mm^3/m and the friction coefficient is 0.2.

Table 2 Orthogonal array (L9) and response table

Sl.No	Material	Applied Load (N)	Sliding distance (m)	Sliding velocity (m/s)	Wear rate (mm^3/m)	Coefficient of friction
1	A1	10	1500	1	0.0136	0.19
2	A1	20	3000	2	0.0109	0.18
3	A1	30	4500	3	0.0254	0.30
4	A2	10	3000	3	0.0097	0.13
5	A2	20	4500	1	0.0102	0.20
6	A2	30	1500	2	0.0026	0.19
7	A3	10	4500	2	0.0068	0.12
8	A3	20	1500	3	0.0124	0.20
9	A3	30	3000	1	0.0161	0.22

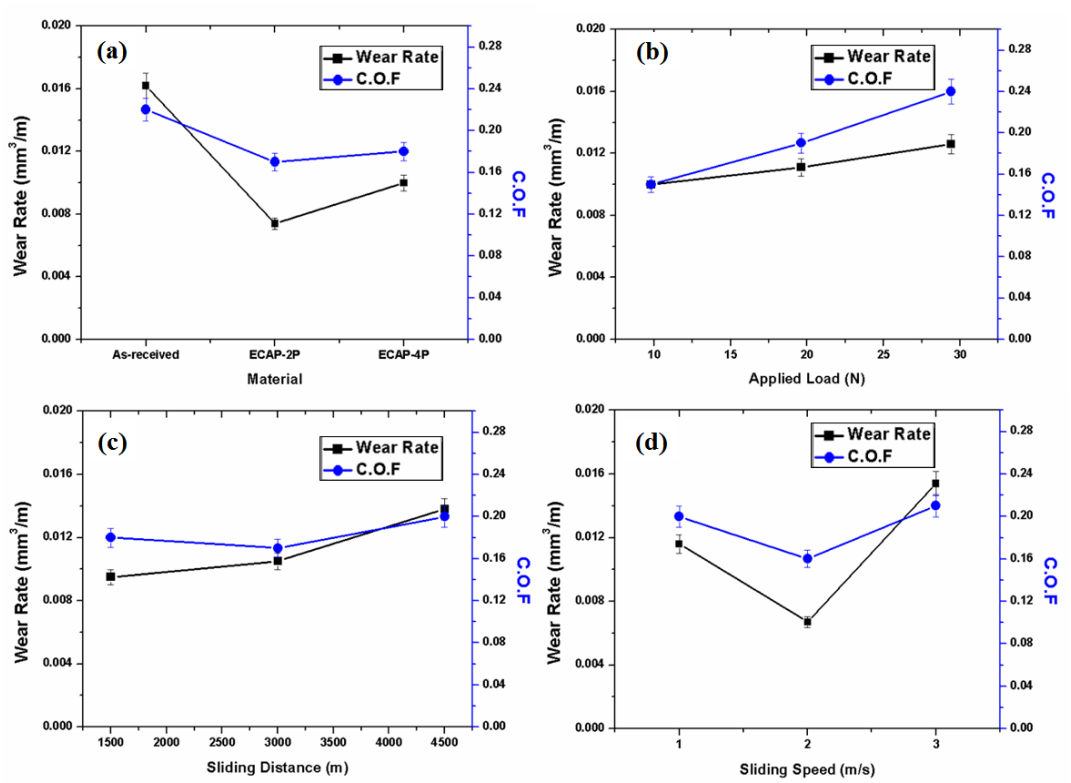

Fig. 4 The effect of individual control parameter on wear rate and coefficient of friction

Curve 3 of Fig. 5 explains the friction coefficient variation under condition A3B1C3D2 (i.e., Expt. No. 7 of Table 2), where the wear rate is 0.0068mm^3/m and the friction coefficient is 0.12. Shows curve 3 is exhibited lower friction coefficient than curve 1 and curve 2 this is more stable because of the higher applied load during dry sliding friction wear, but curve 1 and 2 fluctuated due to the insufficient contact between the pin and the disc surface by the lower applied load. Based on the mean effect plots of wear rate, fine-grained material (Level 2: ECAP-2P), lowest

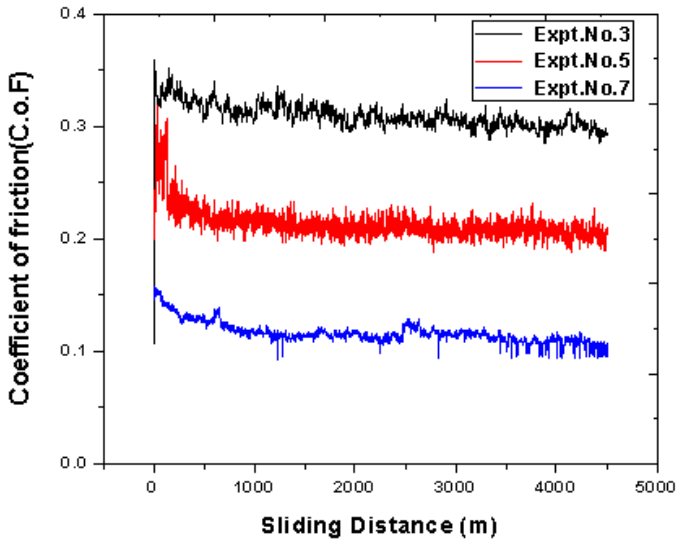

Fig. 5 The coefficient of friction (C.o.F) with respect to sliding distance

Table 3 The response table for wear rate and coefficient of friction

Level	Wear rate (m^3/s)				Coefficient of friction			
	Material	Applied Load (N)	Sliding distance (m)	Sliding speed (m/s)	Material	Applied Load (N)	Sliding distance(m)	Sliding speed (m/s)
1	0.0166	0.0100	0.0095	0.0133	0.2233	0.1467	0.1933	0.2033
2	0.0075	0.0111	0.0122	0.0067	0.1733	0.1933	0.1767	0.1633
3	0.0117	0.0146	0.0141	0.0157	0.1800	0.2367	0.2067	0.2100
Delta	0.0091	0.0046	0.0046	0.0090	0.0500	0.0900	0.0300	0.0467
Rank	1	3	4	2	2	1	4	3

load (level 1: 10N), lowest sliding distance (level 1: 1500m) and medium sliding speed (level 2: 2m/s) are accredited as the optimum setting parameters for minimizing wear rate. In the same manner, the Fig. 4 (a-d). Shows that the fine-grained alloy ECAP-2P, load 10N, sliding distance 3000m and sliding velocity 2.0 m/s acts as the optimal levels for minimizing the coefficient of friction.

Table 3 provided response table for wear rate and coefficient of friction, which shows most influencing factors on wear rate and coefficient of friction. In case of wear rate, material and sliding speed is most influencing parameter followed by applied load and sliding distance. Similarly, for co-efficient of friction applied load and material are the most influencing followed by sliding speed and sliding distance. Table 4 presents the analysis of variance (ANOVA) for the wear rate and coefficient of friction, wherein it is evident that the sliding speed and material influences the wear rate with a percentage contribution of 40.56% and 38.70% respectively to minimize wear rate; whereas applied load and sliding distance have percentage contribution of 10.84% and 9.90%. The applied load (55.87%) and material (20.33%) plays a major role in minimizing the coefficient of friction, whereas sliding speed and sliding distance have the least effect on controlling the coefficient of friction. Also, the experimental results suggest that different modes of wear mechanisms are taking place for the different tested conditions and materials.

Table 4 Analysis of variance (Anova) for wear rate and coefficient of friction

Source	DF	Wear rate (mm^3/m)			Coefficient of friction (C.o.F)		
		Adj. SS	Adj. MS	% contribution	Adj. SS	Adj. MS	% contribution
Material	2	0.000125	0.000062	38.70	0.004422	0.002211	20.33
Applied Load (N)	2	0.000035	0.000018	10.84	0.012156	0.006078	55.87
Sliding distance (m)	2	0.000032	0.000016	9.90	0.001356	0.000678	6.24
sliding speed (m/s)	2	0.000131	0.000065	40.56	0.003822	0.001911	17.56
Error	0	--	--	--	--	--	--
Total	08	0.000323	0.000040	100.00	0.021756	0.002719	100.00

In order to identify the different mechanisms that take place during dry sliding wear of wrought AZ80 Mg alloy, the worn pin was observed under scanning electron microscope. The observations of the worn pin surfaces of magnesium alloy were proven four diverse wear mechanisms working under various wear conditions. They are abrasion, delamination, plastic deformation and oxidation wear mechanism. Fig. 6 (a-d) depicts the aforementioned mixed mode wear mechanism of AZ80 Mg alloy under experimental number #3, #5, #7 and #9 of Table 2. In Fig. 6 (a) it was observed that the small fragment or ribbon-like strips of material is removed during the dry sliding wear process as a result formation of continuous grooves was observed. These grooves are parallel to the pin sliding direction this typical feature is abrasion wear and the growth of subsurface grooves that cause the final detachment. Fig 6 (b), plastic deformation, patches, and cracks are evidently observed and these patch marks and cracks are perpendicular to the pin-sliding direction. This condition is associated with delamination wear mechanism. This is because of improved ductility of the magnesium alloy due to the sudden activation of additional slip planes (Srinivasan *et al*. 2012). An. J *et al*. (2008) and Muhammet *et al*. (2017) described a similar phenomenon in abrasion and delamination wear-mechanism of magnesium alloy respectively. At higher loading condition frictional heating take place during dry sliding between the pin and disc interface, resulting a thin oxide layer is formed. Further, wear occurred due to the removal of oxide fragment causes oxidation wear. Here, prior to material detachment surface became soft due to deformation and cracks creation, this is evidently shown in Fig. 6 (c). These results have similar to those observed in ZE41 Mg alloys (López *et al*. 2011). Fig. 6 (d) shown the worn surface of AZ80 Mg alloy. Scratches, grooves and oxide formation ensue on the contact surface of the pin. An oxide formation is effective in wear mechanism due to low oxidation wear resistance of magnesium alloys. In addition, abrasive wear, delamination a wear mechanism is dominant under higher loads. However, grooves and scratches minimized in ECAP-2P sample compared to as-received and ECAP-4P Mg alloys shown in Fig. 6(b). This has lower wear rate and it showed better wear performance. EDS was studied on worn surfaces of as-received and ECAP 2P samples for experimental trail #3 and #9 of Table 2 as shown in Fig. 6 (a) and (d), respectively. Debris region and oxidation area were subjected to EDS study and it was noticed that oxygen peaks were observable in the region of grooves. Surface oxidation was found on the specimen (Fig 6. (d)) since magnesium and its alloys have a great affinity to oxidation with respect to temperature.

3.4 Electrochemical corrosion study

The electrochemical corrosion behavior of processed and unprocessed wrought AZ80 Mg alloy was characterized by employing potentiodynamic polarization experiments, where a potential

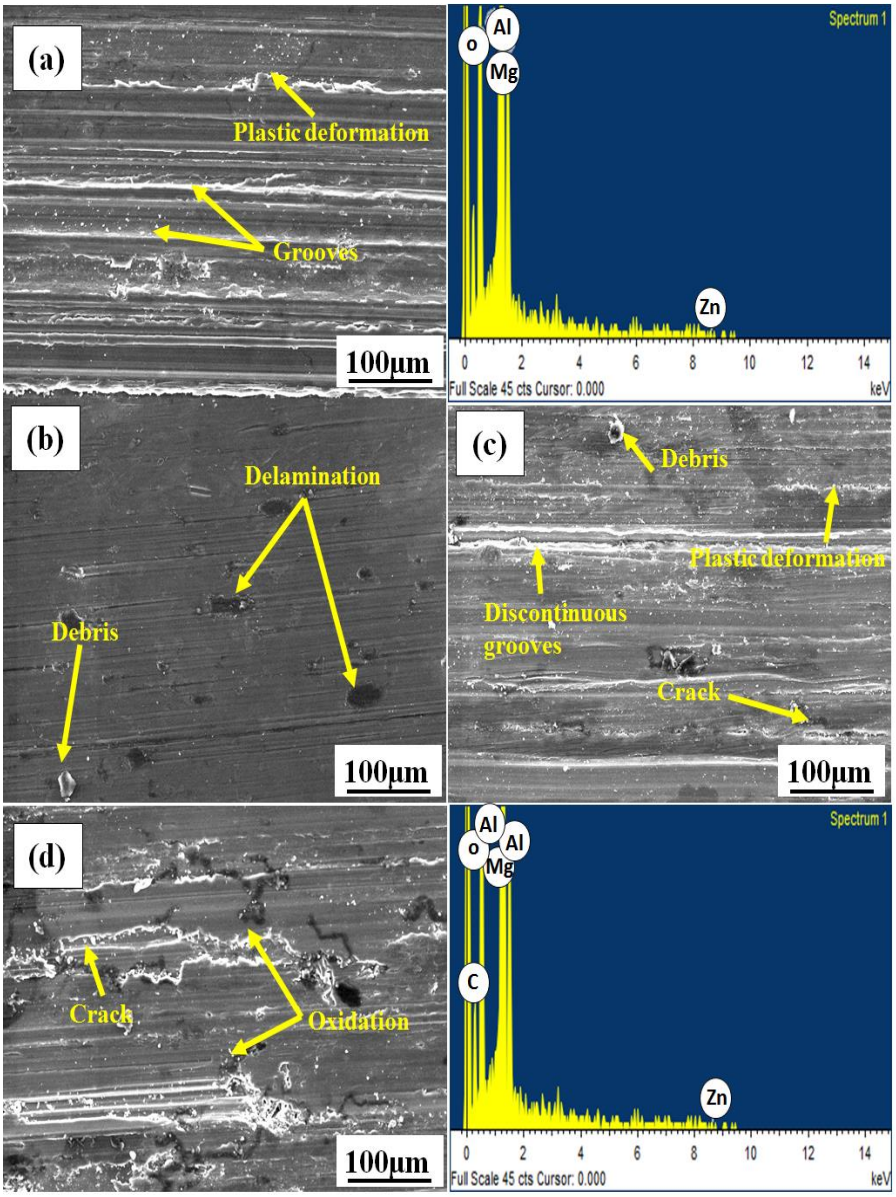

Fig. 6 SEM images of wear mechanism a) Abrasion wear and EDS(Exp.No:#3) b) Delamination (Exp.No:#5) c) Plastic deformation (Exp.No:#7) d) Oxidation wear and EDS (Exp.No:#9)

(V) was applied and the resulting current density was recorded. Fig. 7 illustrates the potential E in V vs. current density i in mA/cm^2 for the as-received and ECAPed wrought AZ80 Mg alloy. Further, potentiodynamic polarization curves for processed and unprocessed wrought Mg alloy was divided into three potential domain such as AB, BC, and CD for the as-received and ECAPed Mg alloy shown in Fig. 7. The domain 'AB' indicates cathodic has potential below -1.53V, -1.48V, -1.42V for as-received, ECAP-2P and ECAP-4P respectively. This specifies corrosion rates were estimated by hydrogen evolution. The active zone 'BC' extends above corrosion potential (E_{corr})

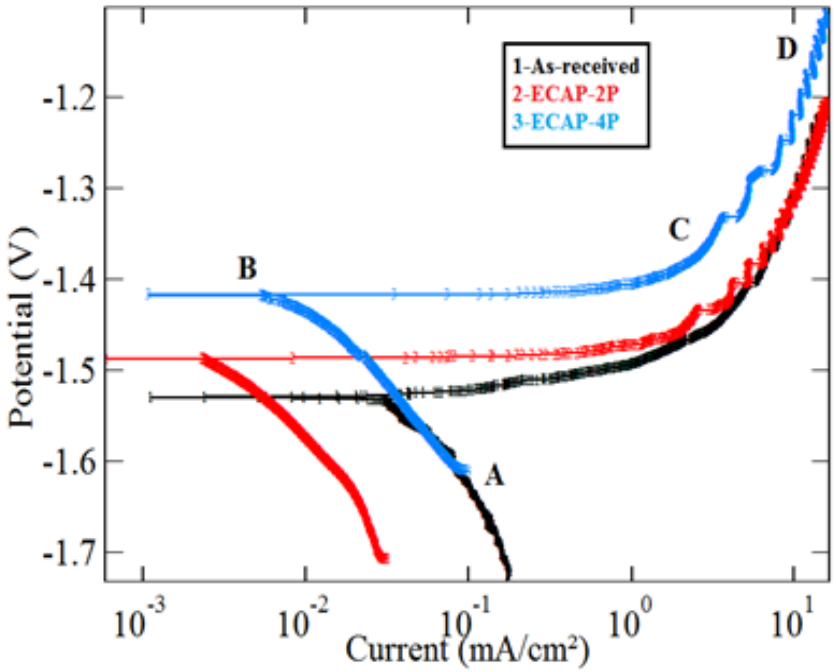

Fig. 7 Polarization plot for as-received and ECAPed AZ80 Mg alloys in 3.5wt.% NaCl solution

and zone 'CD' indicates the passive region. Here, it can be observed that a thin passive oxide layer is formed on the sample surface after the initial period, which is breakdown under the action of chloride content and further re-passivation takes place. This behavior has been observed in zone CD, showed in the form of a wave. The presence of $Mg(OH)_2$ oxide passive layer was confirmed through XRD analysis of corroded sample as shown in Fig. 9 (d). (Gajanan *et al*. 2018). The corrosion potential (E_{corr}) and corrosion current density (i_{corr}), as derived from Tafel slopes, for ECAP-2P are determined to be -1.42 V and 0.02133 mA/cm^2 respectively. Here, ECAP-processed (2P) AZ80 Mg Alloy exhibited better corrosion resistance than the un-processed Mg alloy due to their microstructural changes during ECAP such as finer and more homogeneous grains and secondary phases ($Mg_{17}Al_{12}$) (Figs. 1 and 3).

Nevertheless, the corrosion current density of ECAP-4P sample increased slightly from 0.02133 mA/cm^2 to 0.041517 mA/cm^2. It is because that the multi-pass ECAP creates crystal defects like high dislocation densities and subgrains (Gopi *et al*. 2017). Also obtained UFG exhibited a number of grain boundaries which is act as more anodic this accelerates the dissolution of the working electrode which causes severe corrosion. This mechanism agreed with the previous study (Naiguang *et al*. 2017, Yang *et al*. 2016). Subsequently, ECAP-4P sample contributed slightly improved corrosion potential than ECAP-2P. Because ECAP process distributes the particles of $Mg_{17}Al_{12}$ the potential of these secondary particles is more positive than the α-Mg thus corrosion resistance at E_{corr} is enhanced (Mustafa *et al*. 2012). Fig. 8 (a)-(c) displays the corrosion morphology of the AZ80 Mg alloy investigated in the 3.5 wt.% NaCl electrolyte. It was observed that the as-received Mg alloy show more corrosion pits whereas the as-processed alloy appearances an unaffected surface with less corrosion pits, which shows that the corrosion resistance of ECAP-processed alloy is superior to that of the as-received Mg alloy.

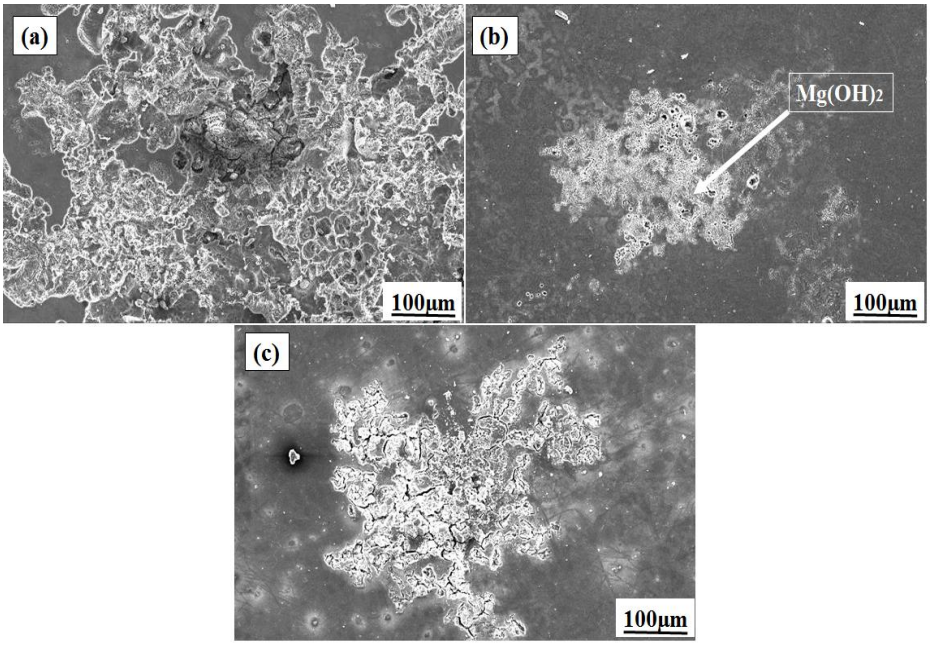

Fig. 8 Corrosion morphology for AZ80 Mg alloys a) as-received b) ECAP-2P c) ECAP-4P

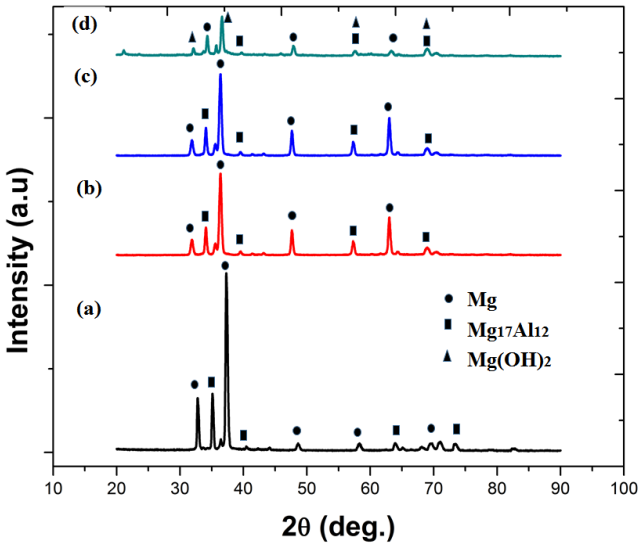

Fig. 9 XRD pattern of a) as-received b) ECAP-2P c) ECAP-4P d) Corroded sample

3.5 XRD analysis

X-ray diffraction results of an AZ80 magnesium alloy of the as-received, ECAP-processed and corroded sample were presented in Fig. 9. From figure, the XRD peaks of the as-received and ECAP-processed alloy consists of Mg and $Mg_{17}Al_{12}$ primary and secondary phases respectively. Also, high intensity peaks are initially observed in the as-received Mg alloy, the intensity of

extruded alloy gradually decreases during ECAP due to shear deformation during ECAP which destroys the texture (FENG *et al*. 2009, Gopi *et al*. 2017). Along with, ECAP-2P corroded sample showed presence of corrosion product Mg $(OH)_2$ depicts in Fig. 9 (d).

4. Conclusions

The experimental investigation and analysis of wear and corrosion behavior of as-received and ECAPed wrought AZ80 Mg alloys contributes the following conclusions:

• ECAP 2 pass processed wrought AZ80 Mg alloys showed increased wear resistance properties as compared to as-received Mg alloy. Wear weight loss of ECAP-2P was reduced by~ 54.4% than that of the as-received condition, the improved wear resistance is due to increased microhardness and grain refinement of the ECAP processed samples. Further lower wear loss values were also observed at 10N load, 1500m sliding distance and 2m/s sliding speed.

• The coefficient of friction (C.o.F) decreased for ECAP-2P sample compared to as-received Mg alloy due to strain handing during sliding and it was lowered at 10N applied load, 3000m sliding distance and 2m/s sliding speed.

• The percentage contribution of input parameters was found from ANOVA table. Material, applied load and sliding speed are found to have the most influence on the wear behavior and coefficient of friction.

• Wear morphology showed the existence of abrasion, delamination, plastic deformation and oxidation wear mechanism. ECAP 2 pass sample demonstrated plane wear surface as compared to as-received condition due to uniform hardness and homogenous microstructure. EDS analysis identified the presence of oxygen (O) and carbon (C) peaks along with magnesium (Mg), aluminium (Al) and zinc (Zn) peaks on the sliding surface.

• Polarization plots revealed better corrosion resistance properties of ECAP 2 pass sample. ECAP 2 pass and 4 pass samples corrosion resistance were improved by 59.23% and 20.63% in comparison to as-received samples respectively. This is due to refined microstructure and uniform distribution of β-phases.

Acknowledgments

This work was supported by DRDO-NRB, Government of India, under grant number NRB/4003/PG/366.

References

An, J., Li, R. G., Lu, Y., Chen, C.M., Xu, Y., Chen, X. and Wang, L.M. (2008), "Dry sliding wear behavior ofmagnesium alloys", *Wear*, **265**(1-2), 97-104.

Bettles, C.J. and Gibson, M.A (2005), "Current wrought magnesium alloys: Strengths and weaknesses", *Jom*, **57**(5), 46-49.

Bolin, H., Yingxia, Y., Songsong, X. and Zongmin, L. (2017), "Effect of ultrasonic impact treating on wear resistanceand microhardness of AZ91D magnesium alloy", *Rare Metal Mat. Eng.*, **46**(1), 17-22.

Esmaily, M., Svensson, J.E., Fajardo, S., Birbilis, N., Frankel, G.S., Virtanen, S., Arrabal, R., Thomas, S. and Johansson, L.G. (2017), "Fundamentals and advances in magnesium alloy corrosion", *Prog. Mater. Sci.*, **89**, 92-193.

Feng, X.M. and Ai, T.T. (2017), "Microstructure evolution and mechanical behavior of AZ31 Mg alloy

processed by equal-channel angular pressing", *Trans. Nonferrous Met. Soc. China*, **19**(2), 293-298.
Gopi, K.R. and Nayaka, H.S. (2017), "Tribological and corrosion properties of AM70 magnesium alloy processed by equal channel angular pressing", *J. Mater. Res.*, **32**(11), 2153-2160.
Gray, J.E. and Luan, B. (2002), "Protective coatings on magnesium and its alloys-a critical review", *J. Alloys Compd.*, **336**, 88-113.
Kulekci, M.K. (2008), "Magnesium and its alloys applications in automotive industry", *J. Adv. Manuf. Technol.*, **39**(9-10), 851-865.
López, A.J., Rodrigo, P., Torres, B. and Rams, J. (2011), "Dry sliding wear behavior of ZE41A magnesium alloy", *Wear*, **271**(11-12), 2836-2844.
Majumdar, J.D., Galun, R., Mordike, B.L. and Manna, I. (2003), "Effect of laser surface melting on corrosion and wear resistance of a commercial magnesium alloy", *Mater. Sci. Eng. A*, **361**(1-2), 119-129.
Naik, G. M. and Narendranath, S. (2018). "Optimization of wire-ed turning process parameters by Taguchi-Grey relational analysis", *i-Manager's J. Mech. Eng.*, **8**(2), 1.
Naik, G.M. and Narendranath, S. (2017). "A parametric optimization of wire-ED turning process parameters on material removal rate of INCONEL 718", *J. Mech. Eng. Biomech.*, **2**(2), 8-14.
Naik, G.M., Gote, G.D. and Narendranath, S. (2018), "Microstructural and hardness evolution of AZ80 alloy after ECAP and post-ECAP processes", *Mater. Today: Proc.*, **5**(9), 17763-17768.
Naik, G.M., Gote, G.D., Narendranath, S. and Kumar, S.S. (2018), "The impact of homogenization treatment on Microstructure Microhardness and Corrosion behavior of wrought AZ80 magnesium alloys in 3.5wt.% NaCl", *Mater. Res. Express*, **5**(8), 086513.
Naik, G.M., Narendranath, S. and Satheesh Kumar, S.S. (2019), "Influence of ECAP processing routes on microstructure mechanical properties and corrosion behavior of AZ80 Mg alloy", *AIP Conf. Pro.*, **2082**, 030016.
Öteyaka, M.Ö., Ghali, E. and Tremblay, R. (2012), "Corrosion behaviour of AZ and ZA magnesium alloys in alkaline chloride media", *J. Corrosion*.
Rusin, N.M., Skorentsev, A.L. and Kolubaev, E.A. (2016), "Dry friction of pure aluminum against steel", *J. Friction Wear*, **37**(1), 86-93.
Shetty, A.S., Akshar, K.S., Prashanth, B.Y. and Naik, G.M. (2017). "Optimization of machining parameters on MRR for EN19 & EN31 steel using Taguchi method", *J. Emerging Res. Manag. Technol.*, 2278-9359.
Srinivasan, M., Loganathan, C., Kamaraj, M., Nguyen, Q.B. and Gupta, M. and Narayanasamy, R. (2012), "Sliding wear behaviour of AZ31B magnesium alloy and nano-composite", *Trans. Nonferrous Met. Soc. China*, **22**(1), 6065.
Taltavull, C., Torres, B., Lopez, A.J. and Rams, J. (2013), "Dry sliding wear behavior of AM60B magnesium alloy", *Wear*, **301**(1-2), 615-625.
Turan, M.E., Sun, Y., Akgul, Y., Turen, Y. and Ahlatci, H. (2017), "The effect of GNPs on wear and corrosion behaviors of pure magnesium", *J. Alloys Compd.*, **724**, 14-23.
Wang, N., Mu, Y., Li, Q. and Shi, Z. (2017), "Discharge and corrosion behavior of AP65 magnesium anode plates with different rolling reductions", *RSC Adv.*, **7**(84), 53226-53235.
Wen, J.L., Yang, Y.K. and Jeng, M.C. (2009), "Optimization of die casting conditions for wear properties of alloy AZ91D components using the Taguchi method and design of experiments analysis", *J. Adv. Manuf. Technol.*, **41,** 430-439.
Yang, Y., Qiao, L., Gao, Z. and Yan, Y. (2016), "Study of wear-corrosion resistance of Co-based biomaterial", *Emerg. Mater. Res.*, **5**(2), 194-200.
Yoshida, Y., Cisar, L., Kamado, S. and Kojima, Y. (2002), "Low temperature superplasticity of ECAE processed Mg-10%Li-1%Zn alloy", *Mater. Trans.*, **43**(10), 2419-2423.
Zhang, X.P, Zhao, Z.P., Wu, F.M., Wang, Y.L. and Wu, J. (2007), "Corrosion and wear resistance of AZ91D magnesium alloy with and without microarc oxidation coating in Hank's solution", *J. Mater. Sci.*, **42**(20), 8523-8528.